



Manipulation of Electromagnetic Waves Via Graphene-Based Coding Metamaterials for Terahertz Applications

Adel Saleeb⁽¹⁾ Ahmed Hassan⁽²⁾ Sayed El-Rabaie⁽³⁾ Ahmed Elkorany⁽⁴⁾

Professor Department of Communications, Faculty of Electronic Engineering, Menoufia University⁽¹⁾

Department of Communications, Faculty of Electronic Engineering, Menoufia University⁽²⁾

Professor Department of Communications, Faculty of Electronic Engineering, Menoufia University⁽³⁾

Associate Professor Department of Communications, Faculty of Electronic Engineering, Menoufia University⁽⁴⁾

*Corresponding author(s). Email: ahmedatef882010@gmail.com

ARTICLE INFO

Article history:

Received:

Accepted:

Online:

Keywords:

Graphene

Coding metamaterials

Terahertz

Scattered wave

ABSTRACT

This paper is concerned with the manipulation of electromagnetic waves in the Terahertz range using graphene. Graphene has the great advantage that its conductivity can be controlled via an electric bias. A unit cell constructed from two square rings enclosing a square patch made of graphene was simulated using HFSS that gives a reflection phase of 0 or π according to the bias. Scattering from a coding metamaterial in the form of a square matrix of 8x8 unit cells was analyzed. A plane wave incident normally on the coding metamaterial is scattered and formed two or four main beams according to the arrangement of unit cells. The unit cells are arranged as groups. The group may be a column or square. The groups alternate as 1x1, which means one group gives zero reflection phase and the next group gives π phase. Arrangements 1x1, 2x2, and 4x4 were studied. The beamwidth and direction of propagation of the scattered beams depend upon the arrangement of the groups (1x1, 2x2, or 4x4). The positions of scattered beamwidths in azimuth are fixed, they do not change with arrangement of groups. The elevation angle of the beams change from large value for 1x1 to smaller value for 4x4. In the limit when all the cells become of the same type, the elevation angle becomes zero and we have only one beam normal to the structure.

1. Introduction

Applications of electromagnetic waves in terahertz frequency range include; wireless communications[1], detection of chemical[2] and biological materials[3], detection of explosives[4] and terahertz (THz) lidar, [5]. Coding metamaterials designed for the microwave range use metallic unit cells. Papers 6, 8, 9, 10, 16, and 17 belong to this category. Coding metamaterials, digital metamaterials, and programmable metamaterials are defined in, [6]. Anisotropic coding metamaterials are used to manipulate differently polarized terahertz waves, [7]. Software defined metamaterials are designed for nanonetworks, [8]. Coding metamaterials of matrix-type are used for the reduction of radar cross section (RCS), [9]. Frequency coding metamaterials are used for controlling energy radiations of electromagnetic waves, [10]. In reference [16], authors obtained multiple functionalities : reconfigurable polarization conversion, beam steering, beam forming and diffusion. The authors of [17] established the concept of reflection-transmission amplitude. They proposed a digital metasurface for full-space electromagnetic manipulations. Paper [18] includes a tutorial material that reviews recent progress in coding metamaterials. It includes survey of the architecture of metasurfaces and discusses the fabrication methods. The paper also shows the applications of metasurfaces in imaging, radar, sensing and communications throughout the whole frequency spectrum from microwaves to optics. Authors of paper [19] provided analysis from computation and communication perspective. This analysis helps the design of controllers integrated within the structure of software-defined metamaterials. This paper also covers the spectrum from microwave to optics.

Revised:27 May, 2022, Accepted:4 June , 2022

Papers 7, 20, 21, and 22 cover the range of terahertz frequencies 0.1 to 10 THz. Paper [20] is an excellent review of progress in wave manipulations by 2D metasurfaces. Paper [21] reviews the macroscale and nanoscale applications of terahertz band communications. Macroscale applications include: 5G cellular networks, terabit wireless local area networks, terabit wireless personal area networks, and secure terabit wireless communications. Nanoscale applications include: health monitoring systems, chemical and biological nano sensors, and the internet of nano things. Paper [21] discussed topics in THz imaging research : time taken to form an image, near-field techniques for subwavelength imaging, and non-destructive investigation of artwork and historical artifacts.

Coding metamaterials require reconfiguring unit cells to construct programmable metasurfaces. Metallic unit cells can be reconfigured using PIN diodes, MEMS switches, liquid crystals, piezoelectric material or varactor diodes. These technologies have their own advantages but suffer from : slow switching time, small dynamic range, limited flexibility and/or high DC bias. Graphene is called 'the wonder material of the 21 century'. This paper considers graphene for the reconfigurability of the coding material. Table 1 compares programmable metamaterial structures from the point of view of frequency range and reconfigurable technique. Graphene is the best reconfigurable technique in THz band.

In this paper the coding metamaterial is made of graphene and the unit cells are arranged in the form of columns or squares. The columns split a plane wave incident normally upon it into two beams and the squares scatters the incident plane wave into four beams. Arrangement of unit cells depends upon the properties of

graphene, [11, 12]. The unit cells are arranged in the form of columns. One column with unit cells that give zero reflection phase, the neighboring column with unit cells that give π reflection phase. This arrangement is referred to as 1x1. Other arrangements 2x2 and 4x4 were studied.

Table 1 Comparison of metasurfaces

Reference	Frequency range	Reconfigurability
6	7 – 14 GHz	Biased diode
8	microwave	CMOS switches
9	6 -15 GHz	N/A
10	6 -11 GHz	Change frequency
16	9 – 12 GHz	PIN diode
17	8.1 – 9.3 GHz	PIN diode
7	THz	Polarization of the wave
20	THz	No reconfigurability
21	THz	Graphene
22	THz	No reconfigurability
This paper	THz	Graphene

This paper is arranged as follows. Section (2) summarizes the properties of graphene. Section (3) presents the unit cell of the coding metamaterial. Different structures of coding metamaterials together with scattered waves are given in section (4). Conclusions are given in section (5).

2. Properties of Graphene

Graphene is carbon-based material, it is a thin two-dimensional single layer of carbon atoms. Graphene has many properties in terms of mechanical strength, mobility, optical transparency, electrical and thermal conductivity [13]. The graphene electrical properties can be tuned by applying suitable external DC voltage. Due to tunable conductivity of graphene it has many applications in Terahertz (THz) range. Graphene supports surface plasmon polarities (SPP) in the THz range.

The silicon-oxide is a more suitable substrate applied for enhancing the graphene layers in THz antenna [14,15]. Graphene can be modelled as an extra thin surface with surface conductivity $\sigma(\omega, \Gamma, \mu_c, T)$ where ω is radian frequency, μ_c is chemical potential, Γ is a phenomenological scattering rate, and T is temperature. For frequencies below 8 THz the conductivity is complex and frequency-dependent and given by:

$$\sigma(\omega, \mu_c, \Gamma, T) \approx -j \frac{q_e^2 K_B T}{\pi \hbar (\omega - j2\Gamma)} X \left(\frac{\mu_c}{K_B T} + 2 \ln(e^{-\mu_c \tau K_B T} + 1) \right) \quad (1)$$

where j refers to the imaginary unit, μ_c is the chemical potential, τ is the relaxation time, K_B is Boltzmann's constant, T is the temperature, ω is radian frequency, $\Gamma = 1/2\tau$ is scattering rate it represents loss mechanism, q_e is the electron charge, and $\hbar = h/2\pi$ is the reduced Planck's constant.

The surface conductivity $Z_s = 1/\sigma$ can be dynamically controlled by applying external bias field.

3. Structure and Simulation of the Unit Cell

The unit cell consists of two square rings and a square patch as shown in Fig.1. The unit cell was simulated using HFSS. The reflection phase was computed as a function of the dimensions of the unit cell and the chemical potential as a parameter. The results are shown in Fig.2. As the chemical potential increases, the

variation of reflection phase with cell dimensions increases. There is nearly no variation of reflection phase for zero chemical potential. For 1 eV chemical potential, the variation of reflection phase reaches 550°. From the figure, the unit cell with dimension $L = 50 \mu\text{m}$ gives zero reflection phase for $\mu_c = 0 \text{ eV}$, and π for $\mu_c = 0.8 \text{ eV}$. The other dimensions of the unit cell are given by :

$$p_x = p_y = \frac{\lambda}{2} = 93.75 \mu\text{m},$$

$$L = 50 \mu\text{m}, w_{c1} = 6.4 \mu\text{m}, w_{c2} = 6.4 \mu\text{m}, g = 4.16 \mu\text{m},$$

$$L1 = L - 2 w_{c1} = 37.2 \mu\text{m}, L2 = L1 - 2 g = 28.88 \mu\text{m},$$

$$L3 = L2 - 2 w_{c2} = 16.08 \mu\text{m}, L4 = L3 - 2 g = 7.76 \mu\text{m}.$$

The substrate was (sio2) with $\epsilon_r = 3.9$. The substrate thickness (h) = 24 μm and operating frequency 1.6 THz.

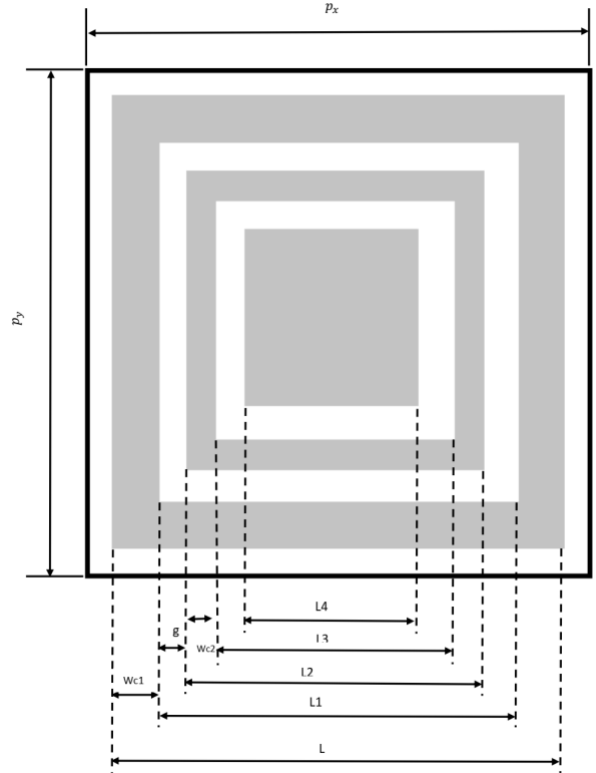


Figure 1: The unit cell

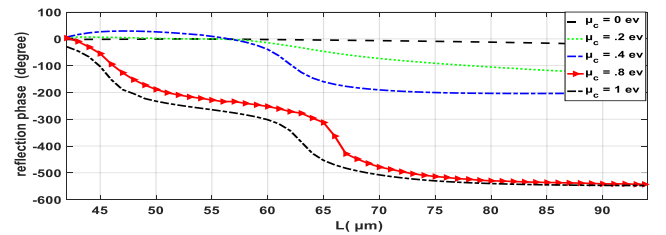


Figure 2: Reflection phase Vs. dimension of the unit cell, the chemical potential is a parameter.

4. The Structure for Manipulating EM Waves

A square metasurface that contains unit cells with dimension D is shown in Fig. (3). The reflection phase $\phi(m,n)$, of each cell

is either 0 or π . When a plane electromagnetic wave is incident normally on the surface, the scattered far field is given by, [6] :

$$f(\theta, \Phi) = f_e(\theta, \Phi) *$$

$$\sum_{m=1}^N \exp(-jkD(m - 0.5)\sin\theta\cos\Phi)$$

$$\sum_{m=1}^N \exp(-jkD(n - 0.5)\sin\theta\sin\Phi) \dots \dots \dots (2)$$

Where $f_e(\theta, \Phi)$ is the pattern of a unit cell. θ and Φ are the elevation and azimuth angles of an arbitrary direction.

4.1. Columns Metasurface

Equation 2 was used for the computation of the scattering patterns of sequences shown in Figs. 4 -7.

A uniform electromagnetic plane wave is incident normal to the surface.

The coding sequence shown in Fig. 4 consists of one column with its elements are 0 phase alternating with one column with its elements have π phase. There are two main beams with elevation angle (θ) equals 35° and azimuth angles $\Phi = 90$ and 270° . To distinguish between the different sequences we call this sequence ‘columns 1x1’.

Figure 5 shows the scattering pattern for a sequence with two 0 columns alternating with two π columns. There are also two main beams with azimuth angles as the previous case, but the elevation angle decreased to 25° . This case is named ‘columns 2x2’.

The case ‘columns 4x4’ is shown in Fig. 6. The two main beams occupy the same azimuth positions, the elevation angle is 10° .

Figure 7 shows the scattered field from a surface in which all unit cells are similar, with 0 reflection phase. There is only one main beam in direction normal to the surface.

The beams of the structure 1x1 are pointing in the direction $\theta = 35^\circ$ away from boresight. The structures 2x2 and 4x4 are pointing at angles 25 and 10 respectively. As the period of the alternating columns increases the elevation angle decreases as shown in Fig. 8. When the period becomes infinite (the case shown in Fig. 7) the elevation angle becomes 0.

The period of alternation of columns has an effect on the beam width. As the period increases the beam width increases as shown in Fig. 9.

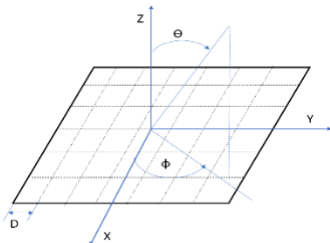


Fig.3 Metasurface with coordinate system

0	π	0	π	0	π	0	π
0	π	0	π	0	π	0	π

0	π	0	π	0	π	0	π
0	π	0	π	0	π	0	π
0	π	0	π	0	π	0	π
0	π	0	π	0	π	0	π
0	π	0	π	0	π	0	π
0	π	0	π	0	π	0	π

Fig. 4a Column arrangement 1x1

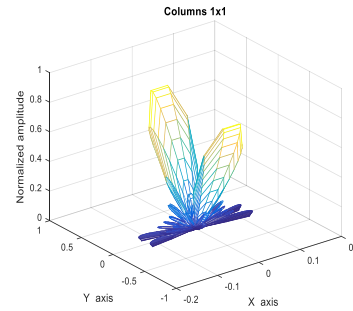


Fig. 4b Radiation pattern structure 1x1

0	0	π	π	0	0	π	π
0	0	π	π	0	0	π	π
0	0	π	π	0	0	π	π
0	0	π	π	0	0	π	π
0	0	π	π	0	0	π	π
0	0	π	π	0	0	π	π
0	0	π	π	0	0	π	π
0	0	π	π	0	0	π	π

Fig. 5a Column arrangement 2x2

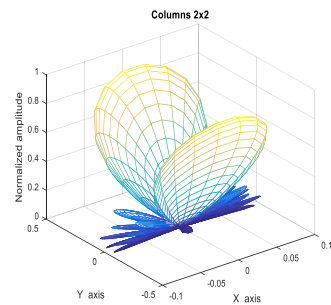


Fig. 5b Radiation pattern structure 2x2

0	0	0	0	π	π	π	π
0	0	0	0	π	π	π	π
0	0	0	0	π	π	π	π
0	0	0	0	π	π	π	π

0	0	0	0	π	π	π	π
0	0	0	0	π	π	π	π
0	0	0	0	π	π	π	π
0	0	0	0	π	π	π	π

Fig. 6a: Column arrangement 4x4

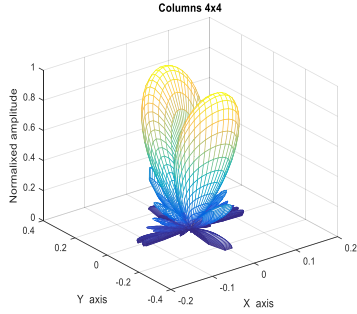


Fig. 6b: Radiation pattern structure 4x4

0	0	0	0	0	0	0	0
0	0	0	0	0	0	0	0
0	0	0	0	0	0	0	0
0	0	0	0	0	0	0	0
0	0	0	0	0	0	0	0
0	0	0	0	0	0	0	0
0	0	0	0	0	0	0	0
0	0	0	0	0	0	0	0

Fig. 7a: All cells are the same

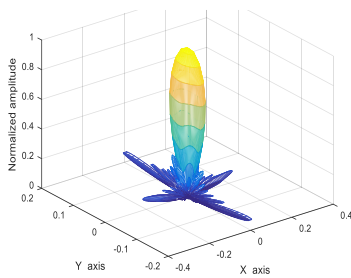


Fig. 7b: Radiation pattern all cells are similar

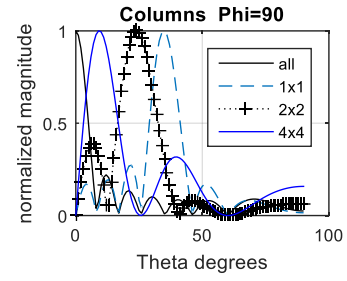


Fig. 8: Effect of period of columns on elevation angle.

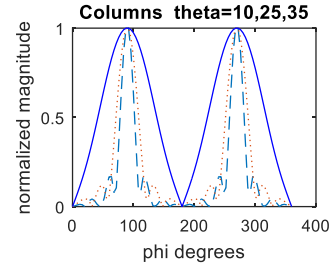


Fig. 9: Effect of period of columns on beamwidth.

4.2. Squares Metasurface

The coding sequence shown in Fig. 10 consists of one unit cell with 0 phase alternating with one unit cell with π phase. There are four main beams with elevation angle (θ) equals 38° and azimuth angles $\Phi = 50, 140, 230$ and 320° . To distinguish between the different sequences we call this sequence ‘squares 1x1’.

Figure 11 shows the scattering pattern for a sequence squares 2x2. There are also four main beams with azimuth angles as the previous case ($\Phi = 50, 140, 230$ and 320°), but the elevation angle decreased to 35° .

The case ‘squares 4x4’ is shown in Fig. 12. The four main beams occupy the same azimuth positions as the previous two cases, the elevation angle is 28° .

The beams of the structure 1x1 are pointing in the direction $\theta = 38^\circ$ away from boresight. The structures 2x2 and 4x4 are pointing at angles 35 and 28 respectively. As the period of the alternating squares increases the elevation angle decreases as shown in Fig. 13. In the limit when the period becomes infinite (the case when all unit cells give the same phase) the elevation angle becomes 0 and we have only one beam. This is the case of Fig. 7.

The period of alternation of squares has an effect on the beam width. As the period increases the beam width increases as shown in Fig. 14. The beamwidths at normalized amplitude equal to 0.5 are 33, 19, and 10° for structures 4x4, 2x2, and 1x1 respectively.

0	π	0	π	0	π	0	π
π	0	π	0	π	0	π	0
0	π	0	π	0	π	0	π
π	0	π	0	π	0	π	0
0	π	0	π	0	π	0	π
π	0	π	0	π	0	π	0

0	π	0	π	0	π	0	π
π	0	π	0	π	0	π	0

Fig. 10a : Squares arrangement 1x1

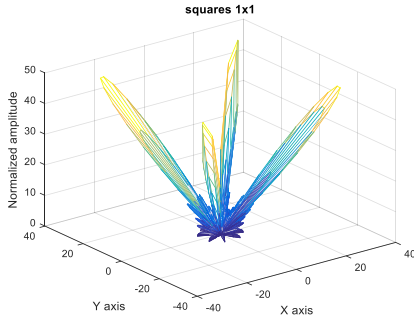


Fig. 10b: Radiation pattern for 1x1 square

0	0	π	π	0	0	π	π
0	0	π	π	0	0	π	π
π	π	0	0	π	π	0	0
π	π	0	0	π	π	0	0
0	0	π	π	0	0	π	π
0	0	π	π	0	0	π	π
π	π	0	0	π	π	0	0
π	π	0	0	π	π	0	0

Fig. 11a: Squares arrangement 2x2

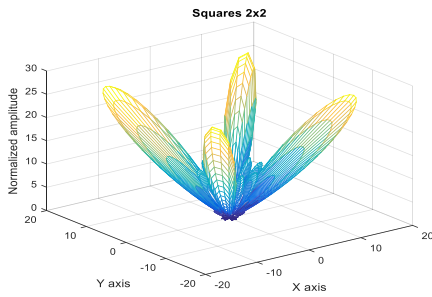


Fig. 11b: Radiation pattern for 2x2 square

0	0	0	0	π	π	π	π
0	0	0	0	π	π	π	π
0	0	0	0	π	π	π	π
0	0	0	0	π	π	π	π
π	π	π	π	0	0	0	0
π	π	π	π	0	0	0	0
π	π	π	π	0	0	0	0
π	π	π	π	0	0	0	0

Fig. 12a: Squares arrangement 4x4

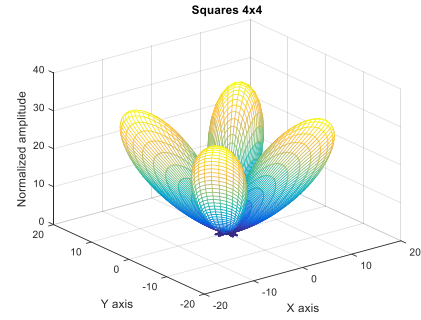


Fig. 12b: Radiation pattern for 4x4 Square

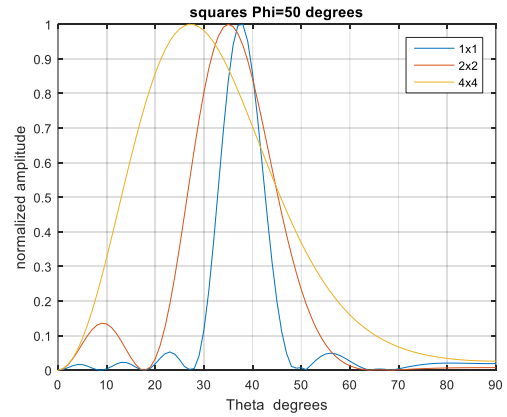


Fig. 13: Effect of period of squares on elevation angle

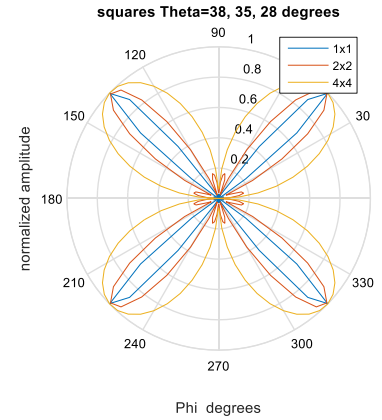


Fig. 14: Effect of period of squares on beamwidth

5. Conclusions

A metasurface consisting of 8x8 unit cells was analyzed. The unit cells were arranged in the form of alternating columns or squares. The alternating columns (or squares) were arranged as 1x1, 2x2 and 4x4. A uniform plane wave incident normally on the structure was scattered with two main beams (for columns arrangement) or four beams (for squares arrangement). The period of the alternating columns affects the directions of the scattered beams in elevation. Table 2 below shows the elevation angle of beams of different arrangements.

Table 2 Elevation angles of scattered beams

Structure	1x1	2x2	4x4
Columns	35	25	10
Squares	38	35	28

As the period increases, the elevation angle of the scattered beams decreases. In the limit when the period becomes infinite the elevation angle approaches zero and we have only one scattered beam normal to the structure. The structure approaches the case of all unit cells are identical. The position in azimuth is not affected. The azimuth angles for the columns arrangement are 90 and 270. While for squares arrangement the azimuth angles are 50, 140, 230, and 320. The period also affects the beamwidth. As the period increases, the beamwidth increases. Table 3 below shows the variation of the beamwidth.

Table 3 Beam width of scattered beams

Structure	1x1	2x2	4x4
Columns	33	50	100
Squares	100	50	33

References

[1] I. Llaster, C. Kremers, A. C. Aparicio, J. M. Jornet, E. Alarcon, and D. N. Chigrin, Graphene-Based Nano Patch Antenna for Terahertz Radiation Elsevier, Photonics and Nanostructures – Fundamentals and Applications, 10 (2012), 353 – 358. <https://doi.org/10.1016/j.photonics.2012.05.011>

[2] C. Han, and I. F. Akyildiz Three-Dimensional End-to-End Modeling and Analysis for Graphene-Enabled Terahertz Band Communications IEEE Trans. On Vehicular Tech. , Vol.66, No.7, July 2017. 10.1109/TVT.2016.2614335

[3] S. H. Zainud-Deen, A. H. Mabrouk, and H. A. Malhat Frequency Tunable Graphene Metamaterial Reflectarray for Terahertz Applications IET, the Journal of Engineering, Vol.2018, Iss. 9, PP.753-761. 10.1049/joe.2018.5016

[4] Z. Chang, B. You, L. S. Wu, M. Tang, Y. P. Zhang, and J. F. Mao A Reconfigurable Graphene Reflectarray for Generation of Vortex THz Waves IEEE Antennas and Wireless Propagation Letters, Vol.15, 2016. 10.1109/LAWP.2016.2519545

[5] Y. Shin, and Y. Zhang Generation of Wideband Tunable Orbital Angular Momentum Vortex Using Graphene Metamaterial Reflectarray IEEE Access, Vol. 6, 2018. 10.1109/ACCESS.2017.2740323

[6] T. J. Cui, M. Q. Qi, X. Wan, J. Zhao, and Q. Cheng Coding Metamaterials, Digital Metamaterials and Programmable Metamaterials Light : Science & Applications, 3, 2014. DOI: 10.1038/lsa.2014.99

[7] S. Liu, T. J. Cui, Q. Xu, and D. Bao Anisotropic Coding Metamaterial and their Powerful Manipulation of Differently Polarized Terahertz Waves Light : Science & Applications, May 2016. DOI: 10.1038/lsa.2016.76

[8] C. K. Liaskos Design and Development of Software Defined Metamaterials for Nanonetworks IEEE Circuits and Systems Magazine, 15 (4), April 2015. DOI: 10.1109/MCAS.2015.2484098

[9] J. J. Yang, Y. Z. Cheng, D. Qi, and R. Z. Gong Study of Energy Scattering Relation and RCS Reduction Characteristics of Matrix-Type Coding Metasurface Applied Sciences Journal, 8, 2018. <https://doi.org/10.3390/app8081231>

[10] H. Wu, S. Liu, X. Wan, and L. Zhang Controlling Energy Radiations of Electromagnetic Waves via Frequency Coding Metamaterials Advanced Sciences, 4, 2017. <https://doi.org/10.1002/advs.201700098>

[11] Arka Karmakar ,Terahertz Hybrid Graphene-Metal Reflectarrays PhD thesis, Faculty of Graduate Studies, The State University of New York, Feb. 2019.

[12] P. Tassin, T. Koschny, and C. M. Soukoulis Graphene for Terahertz Applications Science, Vol. 341, 9 August 2013. DOI: 10.1126/science.1242253

[13] Bin Lin, Zetai Liu, Ying Zhang, Zhipeng Lin, Shaodong Shen, Ping Zheng and Xinyu Wei : ‘The Array Fractal Graphene Antenna Used for Mobile Digital Television’ , 3rd International Conference on Electromechanical Control Technology and Transportation (ICECTT 2018), pp 423-426.

[14] Tuo, Mingguang, : ‘Novel Techniques and Instrumentation for Material Characterization from Microwave to THz Frequencies’ Department of Electrical and Computer Engineering, PhD thesis - The University of Arizona, 2018.

[15] A. Alomainy, K. Yang, M. I. Imran, X. Yao and Q. H. Abbasi eds. Nano-Electromagnetic Communication at Terahertz and Optical Frequencies : Principles and Applications SciTech Publishing, an imprint of IET, 2020.

[16] H. Yang, X. Cao, F. Yang, J. Gao, S. Xu, M. Li, X. Chen, Y. Zhao, Y. Zheng, S. Li, A Programmable Metasurface with Dynamic Polarization, Scattering, and Focusing Control Scientific Reports, Oct. 2016, WWW. Nature.com/scientific reports

[17] R. Y. Wu, L. Zhang, L. Bao, I. w. wu, Q. Ma, G.D. Bai, H. T. Wu, T. J. Cui Digital Metasurface with Phase Code and Reflection-Transmission Amplitude Code for Full-space Electromagnetic Manipulations Adv. Optical Mater. 2019, 7, 1801429

[18] S. Abadal, T. J. Cui, T. Low, J. Georgiou Programmable Metamaterials for Software-defined Electromagnetic Control : Circuits, Systems, and Architectures IEEE Journal on Emerging and Selected Topics in Circuits and Systems, Vol. 10, No. 1, March 2020

[19] S. Abadal, C. Liaskos, A. Tsioliariodm, S. Ioannidis, A. Pitsillides, J. Sole-Pareta, E. Alarcon, and A. C. Aparicio Computing and Communication for the Software-defined Metamaterial Paradigm : A Context Analysis IEEE Access, 2017.

[20] S. W. Qu, H. Yi, B. J. Chen and K. B. Ng, Terahertz Reflecting and Transmitting metasurfaces, Proceedings of IEEE, 2017.

[21] I. F. Akyildiz, J. M. Jornet, and C. Han, Terahertz Band : Next Frontier for wireless Communications, WWW. Elsevier.com /locate / phycom

[22] D. M. Mittleman, Twenty Years of Terahertz Imaging, Optics express, Vol.26, No.8, 2018.